Applied Thermal Engineering 108 (2016) 1237–1242

Contents lists available at ScienceDirect

Applied Thermal Engineering

journal homepage: www.elsevier.com/locate/apthermeng

Research Paper

Numerical study on heat transfer enhancement in capsule-type plate heat exchangers

Yanfeng Zhang, Chen Jiang, Zonglin Yang, Yiyuan Zhang, Bofeng Bai *

State Key Laboratory of Multiphase Flow in Power Engineering, Xi'an Jiaotong University, Xi'an 710049, China

HIGHLIGHTS

- The capsule-type plate heat exchanger is proposed to address high viscosity fluid.
- A unit cell of the capsule-type plate channel is modeled.
- The correlations of friction factor f and Nu are obtained based on the simulation.
- The capsule-type PHE shows a good performance in terms of $Nu/f^{1/3}$.

GRAPHICAL ABSTRACT

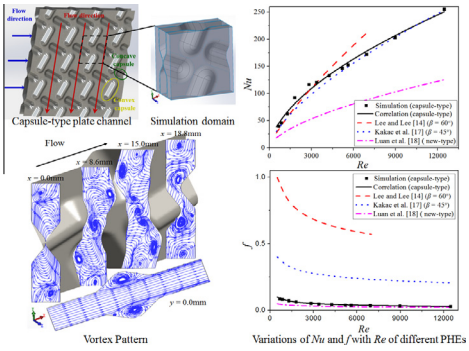

ARTICLE INFO

Article history:
Received 15 April 2016
Revised 3 August 2016
Accepted 4 August 2016
Available online 5 August 2016

Keywords:
Capsule-type plate heat exchanger
Single-phase
Vortex pattern
Correlations
Performance evaluation

ABSTRACT

The capsule-type plate heat exchanger is proposed to address high viscosity fluid which has concave and convex ellipsoidal embossing similar to half capsules. In this paper, single-phase flow and heat transfer in a capsule-type plate channel are investigated numerically. Owing to the periodicity of the structure of the capsule-type plate channel, the heat transfers between the hot and cold fluid in a unit cell with periodic boundary conditions are modeled. Shear Stress Transport k-ω model is employed for turbulent flow. Streamlines, velocity and local convective heat transfer coefficient are presented for discussions. The heat transfer enhancement is found to be primarily attributed to the vortices, one of which has the unique butterfly-shaped head. The correlations of friction factor and Nusselt number in turbulent flow regime with Reynolds number from 500 to 12,470 are obtained based on the simulation results. Compared with other plate heat exchangers (e.g., chevron-type), the capsule-type plate heat exchanger has big Nusselt number, small friction factor f and a good performance with respect to $Nu/f^{1/3}$.

1. Introduction

Plate heat exchangers (PHEs) are widely used in industrial applications such as dairy industry, petroleum industry, chemistry and refrigeration owing to their flexibility, compactness and easy cleaning. But when the working fluid is of high viscosity, serious fouling or clogging may occur. In order to address this problem, in our present study we develop a capsule-type PHE which consists of plates with ellipsoidal embossing similar to a half capsule as shown in Fig. 1. It has the advantages of less deposition and fouling, lower pressure loss and easy cleaning and maintenance in particular compared with the chevron-type PHE and it has been commonly used in petroleum industry. In a capsule-type PHE (see Fig. 1), the straight passages in the channels allow high-pressure water scouring and carrying deposits away without disassembling the plates, which largely simplifies the cleaning and maintenance. However, owing to the complexity of the channel

* Corresponding author.
E-mail address: bfbai@mail.xjtu.edu.cn (B. Bai).

http://dx.doi.org/10.1016/j.applthermaleng.2016.08.033
1359-4311/

Nomenclature

A	area of flow section (m^2)
c	period length
D_e	hydraulic diameter (m)
f	fanning friction factor
h	convective heat transfer coefficient (W/m^2 K)
l	flow length (m)
LV	longitudinal vortex
Nu	Nusselt number
P	perimeter of flow section (m)
PHE	Plate heat exchanger
Pr	Prandtl number
p	pressure (Pa)
q	local heat flux (W)
Re	Reynolds number
r	position coordinates
S	heat transfer area (m^2)
SST	Shear Stress Transport
T	temperature (K)
TV	transverse vortex
u	inlet velocity (m/s)
2D	two-dimensional
3D	three-dimensional

Greek alphabet

β	chevron angle (°)
Δp	pressure drop (Pa)
λ	fluid thermal conductivity (W/m K)
v	kinematic viscosity (m^2/s)
ρ	fluid density (kg/m^3)

Subscripts

a	augmented
ave	average
f	fluid
l	local
w	wall
0	original

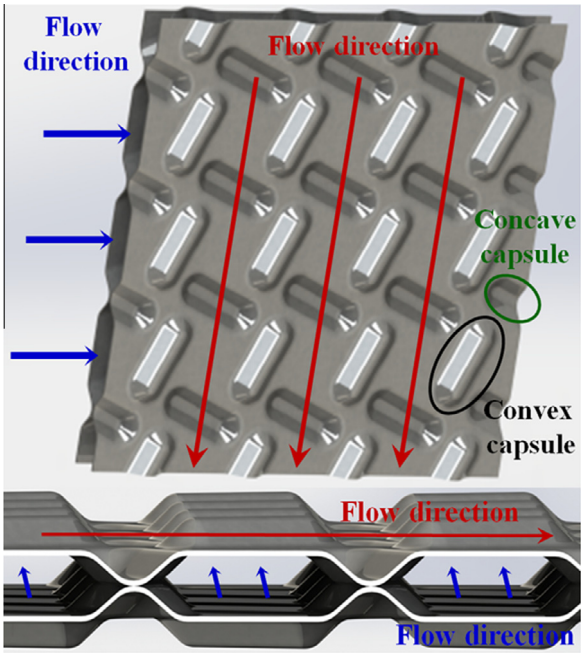

Fig. 1. Schematics of channel and flow arrangement of a capsule-type PHE.

structure, so far few researches have been done on single-phase flow and heat transfer in the capsule-type PHE which, however, are critical qualities in practical applications including operation optimization and structure improvement, etc.

The single-phase flow and heat transfer of chevron-type PHEs have been studied through extensive experiments [1–9] and numerical simulations [10–16]. Nusselt number was found to increase with increasing Reynolds number and chevron angle [1], while other geometrical properties such as port diameter, enlargement factor and channel flow area [2] were also found to have strong influences on thermal and hydraulic performance of heat exchangers. When determining the correlations of friction factor and Colburn factor, Gherasim et al. [4] proposed that pitch and height of chevron be taken into account. Other factors such as surface roughness [6], flow maldistribution [7,8], flow arrangement [10] and fluid viscosity [12] as well as structure of chevron plate were also investigated. The heat transfer coefficient on the ethanol side was found to take higher values with higher surface roughness while that of the water side displayed an opposite tendency. Wajs and Mikielewicz [6] suggested that the difference of surface tension between water and ethanol resulted in this interesting phenomenon. Moreover, many correlations have been proposed for predicting heat transfer and pressure drop of chevron-type PHEs with different structures [9,17], and some of them are verified by experimentation [5]. Compared with these thorough researches on chevron-type PHEs, investigations on other types of PHEs are much less. Luan et al. [18] proposed a new PHE consisting of compound corrugation plates whose heat transfer decreased by 25% and corresponding flow resistance decreased by >50% compared with a traditional chevron-type PHE. Tran et al. [20,21] investigated the flow characteristics and reported a method for geometric design of pillow-plate heat exchangers. Based on his findings on the influences of geometric parameters of capsules on flow and heat transfer, Zhang et al. [22] proposed the optimum structure of capsule-type PHEs.

In this article, commercial software ANSYS CFX is applied to study the single-phase flow and heat transfer in the capsule-type PHE, one new type of PHEs with the advantages of less fouling and easy cleaning. With periodic boundary conditions, a unit cell containing hot and cold fluid and plates is constructed and modeled whose geometry is representative of the structure of the capsule-type plate channels. Streamlines, velocity and local convective heat transfer coefficient are presented to discuss the heat transfer mechanism. The friction factor and Nusselt number are studied as functions of Reynolds number for industrial applications, and the performance evaluation of the heat exchanger is conducted with respect to heat transfer coefficient and pressure drop.

2. Physical and numerical models

2.1. Flow arrangement and geometrical parameters

Fig. 1 shows capsule-type plates with approximately ellipsoidal embossing similar to a half capsule. In the channels of these plates, a cross-current flow is organized, which results in the same flow

and heat transfer for the two working fluids. Moreover, according to the relative position of the channel, the capsules on the plates can be divided into concave capsules and convex capsules, though they have the common structure. Fig. 1 also demonstrates the concave and convex capsules.

As Fig. 2 shows, the main structure parameters are capsule length (22 mm, the length of the rectangle and the two semicircles), capsule width (10 mm, the diameter of the semicircle), capsule height (2.5 mm, the z-axis direction), the angle between concave and convex capsules (90°). Note that the mainstream direction is the array orientation of concave capsules. This results in an included angle between the mainstream direction and its convex capsule direction which equals 24.47°.

2.2. Calculation domain and boundary conditions

To minimize the computational cost, the smallest unit cell, i.e. the region highlighted by the dash-dot-line in Fig. 2, is adopted as the calculation domain considering the periodicity of the capsule-type plate channel. When the planes are set as the periodic boundary conditions, and a fluid particle flows away from one of them, the particle is thus taken as flowing into another plane with equal velocity, pressure, etc. This cell, as Fig. 3 shows, contains three channels of fluids and two plates, where two outside channels compose a whole one as the two outside planes in the z-axis direction are treated with periodic boundary conditions. Besides, periodic boundaries conditions are also employed in both the streamwise and spanwise direction of the hot and cold fluid respectively. For the inside channel, the x-axis is the direction of the mainstream, the y-axis is spanwise and the z-axis plumbs the plates. Note that the two plates in one channel are different technically. The capsules on the back plate show a clockwise trend, while the capsules on the front plate show a counter-clockwise trend as shown in Figs. 2 and 5 respectively. This coupling model containing hot and cold fluid and plates is closer to the physical process than the models under constant heat flux or constant wall temperature conditions. In the calculation, the plates are of stainless steel with the thickness of 0.5 mm, the working fluid is water and no-slip velocity conditions are applied. The flow maldistribution is neglected. For the first period, uniform velocity and uniform temperatures of 60 °C and 20 °C are utilized for the hot and cold fluid respectively at the channel inlets. When the variations of these parameters are equal respectively, it follows that the flow

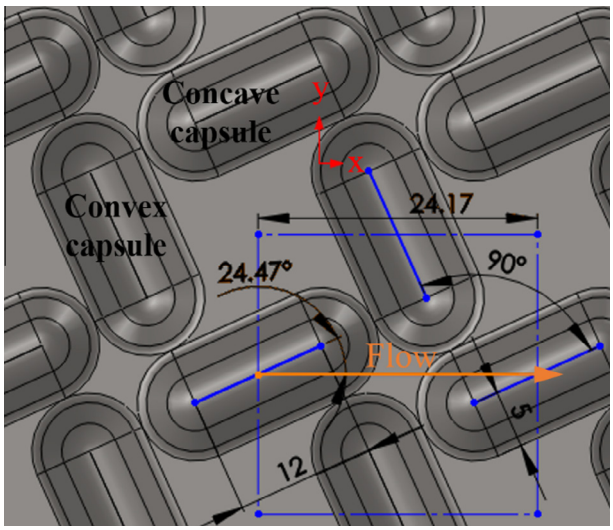

Fig. 2. Schematic of a capsule-type plate.

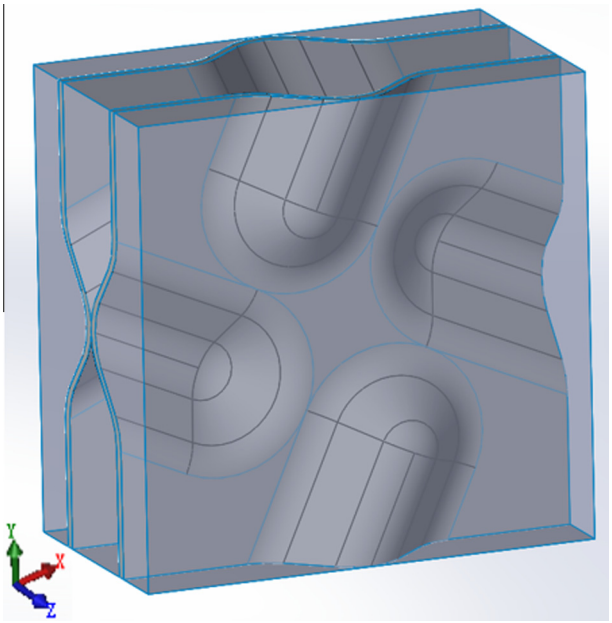

Fig. 3. Calculation domain containing three channels of fluids and two plates.

and heat transfer are fully developed and the data can be analyzed then.

$$\Delta p = p(\boldsymbol{r}) - p(\boldsymbol{r}+c) = p(\boldsymbol{r}+c) - p(\boldsymbol{r}+2c) = \cdots \quad (1)$$

$$h_l(\boldsymbol{r}) = h_l(\boldsymbol{r}+c) = h_l(\boldsymbol{r}+2c) = \cdots \quad (2)$$

2.3. Numerical method

In order to simplify the calculation, the steady incompressible water flow with constant physical properties is applied in this study, and the gravity effect is neglected as well. Reynolds number *Re* of the fluid in this research is between 500 and 12,400. Given that the flow is turbulent when *Re* > 400 in the chevron-type plate channel [15], we assume that the flow in the capsule-type plate channel is also turbulent within the range of Reynolds number in this research. The Shear Stress Transport (SST) k-ω turbulence model is employed to simulate the turbulent flow. The SST k-ω model combines the advantages of both k-ε and k-ω models with activating k-ω model in the near-wall region to forecast the shear flow and k-ε model in the mainstream area to forecast the turbulence flow by employing specific blending functions [23]. Accordingly, the SST k-ω model is able to achieve an accurate description of the turbulence shear stress transmission near the wall and flow separation in the negative pressure region and to avoid over forecasting eddy viscosity of the turbulent flow.

2.4. Data reduction

In this research, Reynolds number is defined as follows:

$$Re = \frac{uD_e}{v} \quad (3)$$

Reynolds number at the inlet section is used to analyze the entire process in this paper. Fanning friction factor is selected to characterize the flow which is defined as follows:

$$f = \frac{\Delta p D_e}{2\rho l u^2} \quad (4)$$

Local convective heat transfer coefficient h_l, average heat transfer coefficient h_{ave} and Nusselt number *Nu* are defined as follows:

$$h_l = \frac{q}{T_w - T_f} \tag{5}$$

$$h_{ave} = \frac{\int h_i dS}{S} \tag{6}$$

$$Nu = \frac{h_{ave} D_e}{\lambda} \tag{7}$$

2.5. Mesh and model validation

The meshes in the whole domain are unstructured tetrahedral elements and generated by ICEM CFD software. To obtain more precise results, the vicinity of the walls is refined with triangular prism meshes and automatic wall-function is adopted. The mesh independence of pressure drop and heat transfer coefficient can be proved as follows. When the number of the elements increases by 26.11%, that is, from 4,296,267 to 5,418,022, pressure drop and heat transfer coefficient increase only by 0.89% and 1.24% respectively. Therefore, the present simulation model with 4,296,267 elements is validated and thus employed in this research.

Ansys CFX is used to analyze the flow and heat transfer in the channel, second-order upwind scheme is selected for convection term and other calculation, with the convergence criteria of RMS residuals of 10^{-5}. Validation of the present numerical model is performed with the experimental data of pressure drop. The experiment is carried out on one channel with two capsule-type plates, the capsule structure of which is the same as that in the simulation. The capsule-type plates are used here without ports and distributions, whose length and width are 610 mm and 168 mm respectively. Deionized water uniformly flows in and out of the plate channel through two distribution headers respectively. The flow flux and the pressure drop are measured by the mass flow meter and the differential pressure transducer, whose accuracies are ±0.1% and ±0.075% respectively. In order to compare the pressure drop in the simulation and the experiment, the pressure drop of a unit cell in the simulation is converted into the pressure drop throughout the channel. As shown in Fig. 4, the simulation results are in good agreement with the experimental values with the maximum error of 8%. Thus the simulation model used in this research proves feasible.

3. Results and discussions

3.1. Vortex pattern

To investigate the vortices of the single-phase flow in capsule-type plate channel, two-dimensional (2D) and three-dimensional (3D) streamlines with *Re* = 3526 are plotted in Figs. 5 and 6 respectively. As the x-axis sections in Fig. 5 shows, a clockwise longitudinal vortex (LV) generates in the downstream of the concave capsules contact point (x = 8.6 mm section) and the counterclockwise LVs generate at the both sides of the clockwise LV (x = 8.6 mm section). Along with the fluid, these LVs decay gradually, while the other two counterclockwise LVs generate at the sides of the concave capsule (x = 18.8 mm section). Moreover, the transverse vortices (TVs) shown in the y-axis section generate in the convex capsules by shearing the action of the wall integrated with the mainstream.

Note that one of the LVs has a complicated structure compared with the conventional LVs. Fig. 6 shows the path line of a fluid particle and the butterfly vortex. This particle flows inversely after it swirls between the two concave capsules and then swirls again

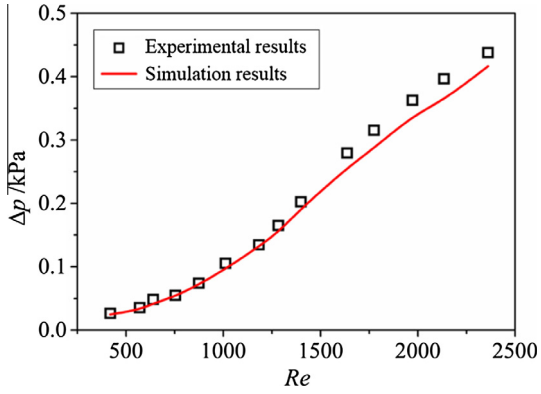

Fig. 4. Pressure drop variation with *Re*: comparison between experimental and simulation results.

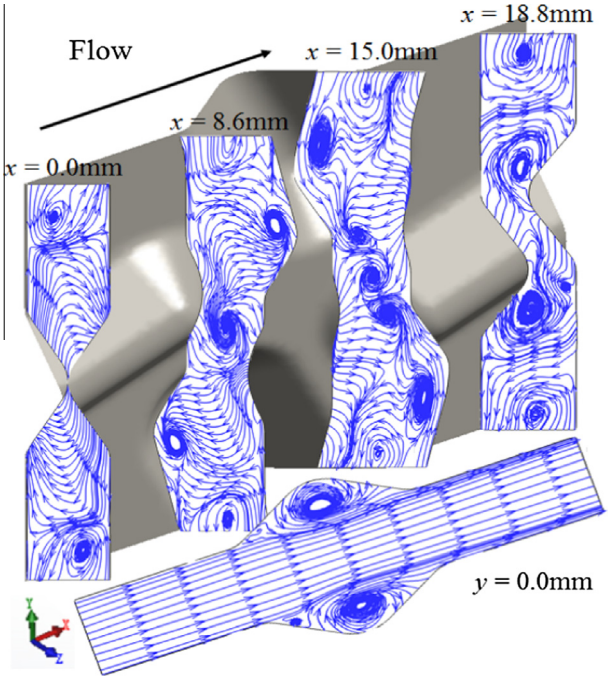

Fig. 5. 2D streamlines of different sections.

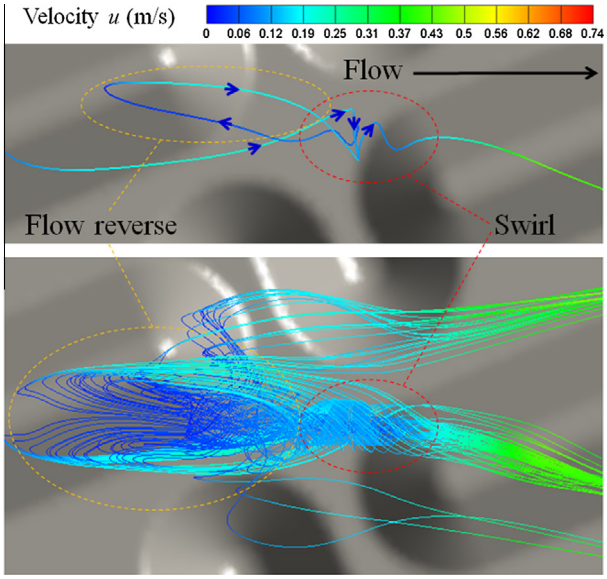

Fig. 6. 3D streamlines of a fluid particle and schematic of butterfly vortex.

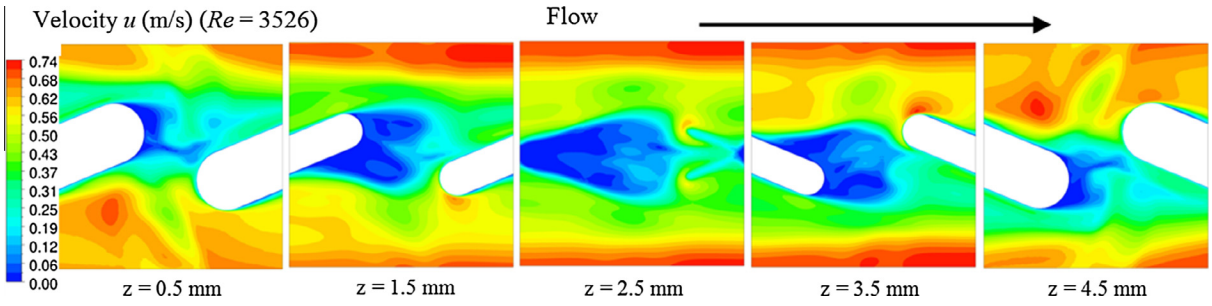

Fig. 7. Velocity distribution of z-axis sections.

in the same region. The lower pressure of the leeside of the concave capsules accounts for this inverse flow. Owing to the different orientations of the concave capsules, the leeside of the concave capsules exhibits rotational symmetry. Thus, the LV has a butterfly-shaped head as Fig. 6 shows.

Therefore, it is concluded that vortices are the major factor of heat transfer enhancement and the capsules play a role similar to that of the vortex generators. Thus, the mechanisms of the vortex generators—the development of boundary layers on vortex generator surface; swirl; and flow destabilization [24]—can also be used to clarify the heat transfer enhancement in capsule-type plate channels.

3.2. Velocity

Fig. 7 shows the velocity of the z-axis sections with $Re = 3526$. The distributions at high Reynolds show nothing representative, thus we show the results at common Reynolds which are much closer to those in industrial applications. Owing to the blocking effect of the concave capsules, flow velocity is lower in this region, while it is higher at the straight passage. Note that the velocity reaches its minimum at the tail of the concave capsules on account of the flow separation.

3.3. Heat transfer characteristics

Fig. 8 shows local convective heat transfer coefficient h_l with $Re = 3526$. h_l reaches its minimum at the tail of the concave capsules owing to the flow stagnation and separation, while h_l is much higher at the upstream concave capsules and the downstream convex capsules, owing to the vortices and the scouring of the fluid.

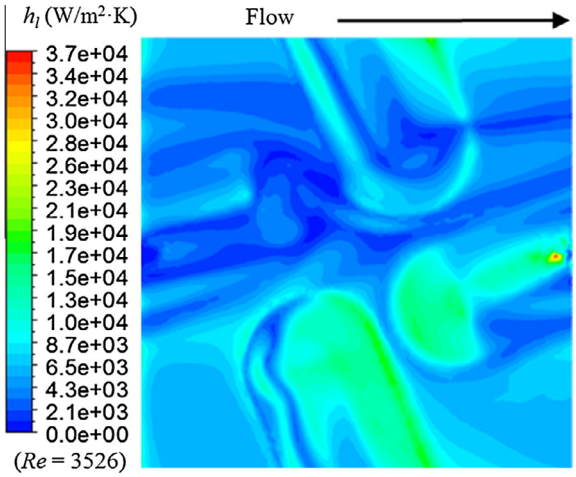

Fig. 8. Distributions of h_l at wall.

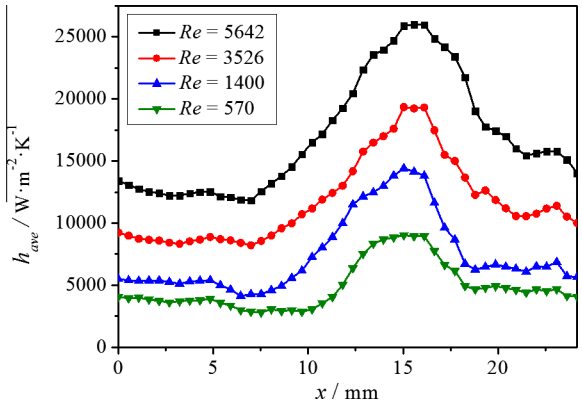

Fig. 9. h_{ave} of different x-axis sections.

Fig. 9 demonstrates h_{ave} on different x-axis sections. When the fluid flows along the concave capsules ($0\ \text{mm} < x < 3\ \text{mm}$), h_{ave} slowly decreases. Then h_{ave} increases slightly ($3\ \text{mm} < x < 5\ \text{mm}$) with LVs starting to generate at the sides of these capsules. And flow separation happens at the tail of the concave capsules, thus h_{ave} slightly decreases again. With the generation of TVs and the scouring of the fluid, h_{ave} reaches the maximum ($12\ \text{mm} < x < 17\ \text{mm}$). Finally, LVs and TVs decay gradually, thus h_{ave} gradually decreases.

4. Performance and evaluation via $Nu/f^{1/3}$

The correlations of Nu and f obtained from the simulation results are as follows:

$$Nu = 0.655\, Re^{0.581}\, Pr^{0.317} \tag{8}$$

$$f = 1.014 Re^{-0.378} \tag{9}$$

The above correlations are valid for Reynolds number from 500 to 12,400 with working fluid of water. The correlations agree well with the simulation results with a maximum deviation of 12.6% of Nu and 6.8% of f and r-square of 0.977 of Nu and 0.994 of f.

To investigate the performance of the capsule-type PHE, variations of Nusselt number and f with Reynolds number of different PHEs are plotted in Fig. 10(a and b) with water as the working fluid. Two chevron-type PHEs with chevron angles β of 45° and 60° respectively which are widely applied and show a good performance and a new type of PHE are chosen. Note that the scope of the correlations of the 45° chevron-type PHE is between 50 and 7000. More information of these three PHEs is available in the corresponding references. Fig. 10(a) shows that the capsule-type PHE has the highest Nusselt number when $Re < 3000$ and the second highest Nusselt number when $Re > 3000$ with its pressure being almost the smallest. Moreover, variations of overheat transfer performance ($Nu/f^{1/3}$) with Reynolds number of different PHEs are

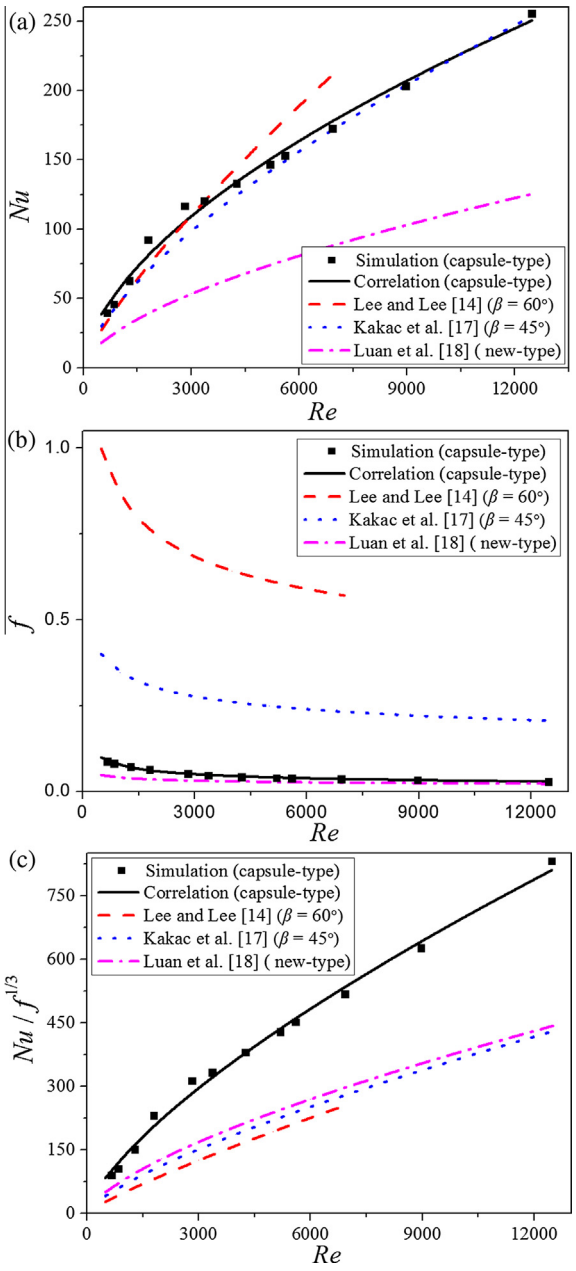

Fig. 10. Variations of (*a*) *Nu*, (*b*) *f* and (*c*) $Nu/f^{1/3}$ with *Re* of different PHEs.

plotted in Fig. 10(*c*). A PHE would have a higher heat transfer rate under the same pumping power consumption if it has a higher $Nu/f^{1/3}$ [25]. Thus, the capsule-type PHE shows a good overheat transfer performance.

5. Conclusions

This work aims to have a profound analysis on the heat transfer enhancement for a single-phase flow in capsule-type PHE. Streamlines, velocity and local convective heat transfer coefficient are presented. The longitudinal and transverse vortices in capsule-type plate channels are the main factors of heat transfer enhancement. Particularly, the butterfly vortex which is formed by the shape and arrangement of concave capsules, is found. Vortices and the scouring of the fluid result in a higher heat transfer coefficient in the upstream of concave capsules and the downstream of convex capsules. The correlations of friction factor *f* and Nusselt number in turbulent flow regime with Reynolds number from 500 to 12,470 are obtained based on the simulation results. Compared with other PHEs, the capsule-type PHE has big Nusselt number and slight pressure drop. Consequently, it shows a good performance with respect to $Nu/f^{1/3}$.

Acknowledgement

This work was supported by the China National Funds for Distinguished Young Scientists (51425603).

References

[1] T.S. Khan, M.S. Khan, M.C. Chyu, Z.H. Ayub, Experimental investigation of single phase convective heat transfer coefficient in a corrugated plate heat exchanger for multiple plate configurations, Appl. Therm. Eng. 30 (2010) 1058–1065.
[2] C. Gulenoglu, F. Akturk, S. Aradag, N.S. Uzol, S. Kakac, Experimental comparison of performances of three different plates for gasketed plate heat exchangers, Int. J. Heat Mass Transf. 75 (2014) 249–256.
[3] T.S. Khan, M.S. Khan, Z.H. Ayub, Experimental investigation of single-phase heat transfer in a plate heat exchanger, J. Therm. Sci. Eng. Appl. 7 (2015). 044501-3.
[4] I. Gherasim, M. Taws, N. Galanis, C.T. Nguyen, Heat transfer and fluid flow in a plate heat exchanger part I: experimental investigation, Int. J. Therm. Sci. 50 (2011) 1492–1498.
[5] A. Yildiz, M.A. Ersöz, Theoretical and experimental thermodynamic analyses of a chevron type heat exchanger, Renew. Sustain. Energy Rev. 42 (2015) 240–253.
[6] J. Wajs, D. Mikielewicz, Influence of metallic porous microlayer on pressure drop and heat transfer of stainless steel plate heat exchanger, Appl. Therm. Eng. 93 (2016) 1337–1346.
[7] B.P. Rao, S.K. Das, An experimental study on the influence of flow maldistribution on the pressure drop across a plate heat exchanger, ASME J. Fluids Eng. 126 (2004) 681–691.
[8] B.P. Rao, B. Sunden, S.K. Das, An experimental investigation of the port flow maldistribution in small and large plate package heat exchangers, Appl. Therm. Eng. 26 (2006) 1919–1926.
[9] D. Dovic, B. Palm, S. Švaic, Generalized correlations for predicting heat transfer and pressure drop in plate heat exchanger channels of arbitrary geometry, Int. J. Heat Mass Transf. 52 (2009) 4553–4563.
[10] F.C.C. Galeazzo, R.Y. Miura, J.A.W. Gut, C.C. Tadini, Experimental and numerical heat transfer in a plate heat exchanger, Chem. Eng. Sci. 61 (2006) 7133–7138.
[11] K. Sarraf, S. Launay, L. Tadrist, Complex 3D-flow analysis and corrugation angle effect in plate heat exchangers, Int. J. Therm. Sci. 94 (2015) 126–138.
[12] I. Gherasim, N. Galanis, C.T. Nguyen, Effects of dissipation and temperature-dependent viscosity on the performance of plate heat exchangers, Appl. Therm. Eng. 29 (2009) 3132–3139.
[13] J. Lee, K.S. Lee, Flow characteristics and thermal performance in chevron type plate heat exchangers, Int. J. Heat Mass Transf. 78 (2014) 699–706.
[14] J. Lee, K.S. Lee, Friction and Colburn factor correlations and shape optimization of chevron-type plate heat exchangers, Appl. Therm. Eng. 89 (2015) 62–69.
[15] I. Gherasim, M. Taws, N. Galanis, C.T. Nguyen, Heat transfer and fluid flow in a plate heat exchanger part II: assessment of laminar and two-equation turbulent models, Int. J. Therm. Sci. 50 (2011) 1499–1511.
[16] M. Kan, O. Ipek, B. Gurel, Plate heat exchangers as a compact design and optimization of different channel angles, Acta Phys. Pol. A 128 (2-B) (2015).
[17] S. Kakac, H.T. Liu, A. Pramuanjaroenkij, Heat Exchangers Selection, Rating and Thermal Design, third ed., CRC Press, Florida, 2012.
[18] Z.J. Luan, G.M. Zhang, M.C. Tian, M.X. Fan, Flow resistance and heat transfer characteristics of a new-type plate heat exchanger, J. Hydrodyn. 20 (2008) 524–529.
[20] J.M. Tran, M. Piper, E.Y. Kenig, Experimental investigation of convective heat transfer and pressure drop in pillow plates under single-phase through-flow conditions, Chem. Ing. Tech. 87 (2015) 3226–3234.
[21] M. Piper, A. Olenberg, J.M. Tran, E.Y. Kenig, Determination of the geometric design parameters of pillow-plate heat exchangers, Appl. Therm. Eng. 91 (2015) 1168–1175.
[22] Y.F. Zhang, P. Xiao, C. Xie, Z.L. Yang, B.F. Bai, The effect of the structure of bubble type plate element on heat transfer, J. Eng. Therm. 36 (2015) 90–92.
[23] A.G. Kanaris, A.A. Mouza, S.V. Paras, Flow and heat transfer prediction in a corrugated plate heat exchanger using a CFD code, Chem. Eng. Technol. 29 (2006) 923–930.
[24] M. Fiebig, Embedded vortices in internal flow: heat transfer and pressure loss enhancement, Int. J. Heat Fluid Flow 16 (1995) 376–388.
[25] J.F. Fan, W.K. Ding, J.F. Zhang, Y.L. He, W.Q. Tao, A performance evaluation plot of enhanced heat transfer techniques oriented for energy-saving, Int. J. Heat Mass Transf. 52 (2009) 33–44.